Optimization of sonication-assisted synthesis of magnetic *Moringa oleifera* as an efficient coagulant for palm oil wastewater treatment

Mohamed Hizam Mohamed Noor [a], Muhammad Faiz Zaim Mohd Azli [a], Norzita Ngadi [a,*], Ibrahim Mohammed Inuwa [b], Lawal Anako Opotu [c], Mahadhir Mohamed [a]

[a] *School of Chemical and Energy Engineering, Faculty of Engineering, Universiti Teknologi Malaysia, 81310 Skudai, Johor, Malaysia*
[b] *Department of Industrial Chemistry, Kaduna State University, Nigeria*
[c] *Department of Applied Chemistry, College of Science and Technology, Kaduna Polytechnic, Nigeria*

ARTICLE INFO

ABSTRACT

Optimization of the sonication-assisted synthesis of magnetic *Moringa oleifera* (MMO) was carried out, to produce an efficient coagulant for palm oil mill effluent treatment. Response surface methodology (RSM) was used to analyse the effect of magnetic nanoparticles (MNPs) composition, sonication time and sonication temperature on coagulation performances to remove total suspended solid (TSS), colour, chemical oxygen demand (COD) and sludge volume index (SVI)). The RSM analyses indicate 1.0 wt% of MNPs, 2.35 min and 50 °C as the optimal MNPs mass fraction, sonication time and sonication temperature, respectively in order to fabricate an efficient MMO coagulant. The analysis of variance (ANOVA), indicate that mass fraction of MNPs and sonication temperature are the most significant parameters. From the statistical analysis, the sonication time did not exert any influence on the fabrication of MMO as well as its coagulation performance. At the optimum conditions, 83.3%, 28.1%, 85.2% removal of TSS, colour, COD as well as 485 mL/g of SVI were respectively achieved. This paper also present the characterization studies on the synthesized MMO using Fourier transform infrared spectroscopy, X-ray diffractometry, scanning electron microscopy and vibrating sample magnetometer analysis.

1. Introduction

Since it was first discovered in 1794 by biologist, Lazzaro Spallanzani, ultrasound technology has evolved from day-to-day and receiving a great contribution in various area of studies (Luo et al., 2005). In medical and clinical fields, wide application of ultrasound technology is found in radiology medical imaging, diseases diagnostic etc (Mace et al., 2013). In engineering line, it was involved in sensor and electronic devices manufacturing (Sudol, 2010), materials and nanomaterials science (Dai et al., 2020; Yang et al., 2020). The application of ultrasound also has root in wastewater treatment technology and for contaminants remediation and this 'green' technology hold a promising future prospects (Wu et al., 2013; Zhou et al., 2020). Contrary to conventional methods, ultrasound technology may offer advantages such

as environmental friendliness (because no toxic chemicals are consumed or produced), low costs (in small-scale) and compact (because the method allows on-site treatment) (Pham et al., 2013).

As a part of hierarchy in most of wastewater treatment plant, coagulation–flocculation (C–F) is a well-known type of treatment process due to its simplicity and low operating cost in the solid–liquid separation and degradation of colloidal pollutants (Wongcharee et al., 2020). The objective of this process is to aggregate or agglomerate together a finely divided or dispersed particles (e.g dissolved solids, colloids or organic matter) than remain suspended in the water to form large particles of such a size (flocs) which settle and cause clarification of the system by means of addition of C–F agents (Lee et al., 2014). Aluminium sulphate (or alum), ferric chloride, polyaluminium chloride (PAC) are some examples of conventional coagulants that are commonly used in treating wastewater due to its availability and satisfactory performance. However, these coagulation agents require process condition alteration (e.g. pH, alkalinity) and generate voluminous metallic sludge which can cause environmental and health effects (Camacho et al., 2017). Researchers are searching for a more sustainable and eco-friendly natural coagulants to substitute the existing coagulants. *Moringa oleifera* (*M.oleifera*) seeds are potential candidates beside cellulose, chitosan, tannin etc. (de Paula et al., 2018).

The seeds of *M.oleifera* contain cationic protein of high molecular weight which may act as water clarifying agent and since *M.oleifera* seed is a natural source, the sludge produced at post-treatment are organic and nontoxic compared to the usage of inorganic coagulants (Baptista et al., 2015). The performance of *M.oleifera* as coagulant, in particular, is well documented as an effective coagulation agent in treating various type of liquid effluents which include textile wastewater (Pecora et al., 2018), concrete plant wastewater (de Paula et al., 2018), municipal wastewater (Garcia-Fayos et al., 2016) and agro-wastewater (Bhatia et al., 2007; Garde et al., 2017). Besides, many studies have already enhanced *M.oleifera* coagulation activity such as preparing its extract with saline solutions (Madrona et al., 2010) and recently studies on functionalized magnetic nanoparticles (MNPs) brings an interesting innovative research direction (Villaseñor Basulto et al., 2018).

The functionalization of MNPs with *M.oleifera* seeds or its extract is very appealing mainly due to its various benefits, such as high efficiency, downsizing the use of chemical products, speedy settling time of flocs due to magnetic characteristics and low cost materials (Lakshmanan and Kuttuva Rajarao, 2014). In producing magnetic *M.oleifera* coagulant (MMO), Santos et al. (2016) employed ultra-sonication technology and from the finding from characterization studies, it is proven that MNPs successfully composite onto the *M.oleifera* surface. The same synthesis procedure was also followed by Mateus et al. (2018a,b). The study focused on the relevant mechanism in pollutants degradation and results showed that the C–F/ adsorption mechanism are largely influenced by the pH nature. Reck et al. (2019) in another study successfully proved that *M.oleifera* functionalized with MNPs hastened the settlement of Reactive Black 5 (RB5) dye particles and their separation. Recently, Triques et al. (2020) performed a C–F test on effluent from dairy industry, and they found out that MMO shortened the settling time and became advantageous when the sludge produced are more compact and less toxic when ecotoxicology tests were conducted. Above all the published works on methodology to synthesis MMO and its prominence efficiency as coagulant, none of these research reports on the effect of preparation conditions especially focused on ultra-sonication conditions with respect to the effect of sonication time, sonication temperature, sonication frequency etc. during synthesis of MMO. Moreover, optimization study of these process conditions may give a better outlook in producing a highly effective product.

Therefore, the objectives of this study were: (i) to apply response surface methodology (RSM) with Box–Behnken Design (BBD) to optimize ultrasound-synthesis of MMO coagulant; (ii) to reveal possible physical characteristics that maybe related to coagulation performance by characterizing an optimized synthesized MMO coagulant. The optimized MMO was selected through a coagulation test on removing selected parameters from palm oil mill effluent (POME), known as high-strength wastewater generated from palm oil industry that contain high colloidal organic contaminants which made it suitable for the present study.

2. Materials and methods

2.1. Materials and POME collection

Magnetite powder and calcium chloride (CaCl$_2$, 96% purity) were purchased from Inoxia Ltd., UK and Bendosen Laboratory Chemicals, Malaysia, respectively. *M.oleifera* seed were purchased from Nutropure, China. The seeds were de-husked and crushed using blender before sieving through a 2 mm-mesh and stored inside container under temperature of 7–12 °C to maintain freshness and dryness for further use.

The POME samples used in this study were obtained from a palm oil mill site located in the city of Bandar Penawar, Johor, Malaysia with temperature ranging between 40 and 50 °C. For preservation of sample, the collected samples were kept in refrigerator at temperature of 4 °C to prevent microbial actions. Due to inconsistent quality of collected POME over time, therefore, the initial parameter values of fresh POME in different sets of experiment were determined and recorded in order to obtain the mean parameter values. The characteristics of POME were as follows: pH of 8.49 ± 0.30, total suspended solid (TSS) of 120.25 ± 9.25 mg/L, colour of 3,592.0 ± 10.4 PtCo, turbidity of 65 ± 5 NTU and chemical oxygen demand (COD) of 16,405.1 ± 61.4 mg/L. It is best to mention that the sample collection and characterization of sample POME were conducted according to standard methods (APHA et al., 1992) as explained in Section 2.2.3.

2.2. Experimental procedure

2.2.1. Ultra-sonication synthesis of MMO coagulant

Prior to synthesis of MMO coagulant, *M.oleifera* extract solution was firstly prepared. 3 g of *M.oleifera* seed powder was mixed with 0.1 L of 0.5M $CaCl_2$ and then allowed the extraction of active component process to proceed by stirring at 100 rpm for 30 min. These were the best conditions obtained based on our preliminary experiments (Mohamed Noor et al., 2021). After stirring, the mixtures were filtered and the filtrate which was 3wt% *M.oleifera* extract solution, was stored in the refrigerator with temperature ranging from 7–12 °C.

The synthesis of MMO coagulant was performed in ultra-sonicator (Model: WUC-A03H, PMI-Labortechnik GmbH, Grafstal). Different MNPs mass fraction were mixed with 0.1 L of 3wt% *M.oleifera* extract solution and then subjected to different sonication time and sonication temperature according to experimental design provided by RSM as shown in Section 2.2.4. After the ultra-sonication process was completed, the mixture was filtered through qualitative filter paper. The MMO coagulant powder was dried at 60 °C in the air drying oven until a constant weight was obtained.

2.2.2. Coagulation procedure by jar test

The series of jar test experiments were conducted on the prepared MMO coagulant using flocculator (Model: SJ-10, Thrusoft Med Co., Ltd., South Korea). Briefly, 1 g of MMO coagulant was added to a litre of POME. Rapid mixing was done at 150 rpm at first 2 min followed by slow mixing at 30 rpm for 30 min. The mixture was transfer to 1 L measuring cylinder and remained undisturbed for 15 min to allow the settlement of flocs. The supernatant was collected to proceed with chemical analysis as explained in Section 2.2.3 and the volume of settled flocs were recorded.

2.2.3. Determination of response

The removal efficiency of TSS, colour, COD was determined by using Eq. (1):

$$Percentage\ removal\,(\%) = \frac{C_i - C_f}{C_i} \times 100 \tag{1}$$

Where C_i and C_f were defined as initial and final concentrations of each substance, respectively.

TSS analysis was conducted according to APHA 2540D method, whereby a fixed volume of supernatant was filtered and dried at 103–105 °C for 2 h. The weights of filter paper before and after filtration were recorded. Then, TSS content was calculated based on Eq. (2):

$$mg\frac{TSS}{L} = \frac{(a - b) \times 1000}{sample\ volume,\ mL} \tag{2}$$

Where a denotes weight of filter paper and b denotes weight of dry filter paper after filtration, measured in gram.

Colour of supernatant before and after treatment was analysed according to APHA 2120 standard method by using HANNA COD Meter and Multiparameter Photometer (HI 83099). Meanwhile, COD analysis was conducted according to APHA 5220D standard closed reflux, calorimetric method. Lastly, APHA 2710D standard method was applied to measure the SVI, according to Eq. (3).

$$SVI\left(\frac{mL}{g}\right) = \frac{settled\ sludge\ volume\left(\frac{mL}{L}\right) \times 1000\frac{mg}{g}}{TSS\left(\frac{mg}{L}\right)} \tag{3}$$

Where settled sludge volume was recorded after sedimentation time end and TSS was measured according to Eq. (2).

2.2.4. Statistical optimization using RSM

The RSM was applied to formulate computationally the effect of variables and their interaction in a model system, which is useful for determination of an optimal combination of multiple variables, while it cuts the total number of experimental trials (Zhou et al., 2018). In this study, the BBD, as a standard design of RSM, was used to optimize the experimental parameters. The MNPs mass fraction (A), sonication time (B); and sonication temperature (C) were independent variables, with levels given in Table S1 (Supplementary Materials). The percentage removal (%) of TSS, colour and COD as well as sludge volume index (SVI) was dependent variables and denoted as Y1, Y2, Y3 and Y4, respectively. 17 runs including replicates at the central point were tested, whose settings are tabulated in Table S2 (Supplementary Materials).

Design-Expert software version 6.0.4 (Stat-Ease, Inc., USA) was used for the analysis of variance (ANOVA) as well as to analyse the interaction between independent and dependent variables and to plot response surfaces. The responses were fitted using a polynomial quadratic equation to correlate it with independent variables, as shown in general Eq. (4):

$$Y = A_0 + \sum_{i=1}^{3} A_i X_i + \sum_{i=1}^{3} A_{ii} X_i^2 + \sum_{i=1}^{2} \sum_{j=i+1}^{3} A_{ij} X_i X_j \tag{4}$$

Where Y is the response, A_0 is a constant, A_i are the coefficients for linear terms, A_{ii} and A_{ij} are the coefficients for quadratic terms, X_i and X_j are the values of studied factors.

2.3. Characterization of MMO coagulant

Once the optimum conditions of synthesized MMO were determined, the structural and morphological analyses were performed. The functional groups of MMO were determined using Fourier transform infrared (FTIR) spectrometer (Model: IRTracer 100, Shimadzu, Malaysia). Then, the crystalline structural characteristics of MMO were recorded using X-ray diffractometer (XRD) (Model: SmartLab X-ray Diffractometer, Applied Rigaku Technologies, Inc, USA) using the following conditions: voltage 40 kV; current 30 mA; filter: monochromatic Cu K "beta" radiation; wavelength: 0.139225 nm; scanning from angle $2\theta = 0$–$100°$ with a step size and step time of $0.01°$ and 2 s, respectively. The morphological behaviour of samples were also examined by scanning electron microscopy (SEM) (Model: TM3000, Hitachi, Japan). The samples, sprinkled sparsely over aluminium stub, were metallized by depositing a thin layer of platinum (20 mm thick) on the surface using a SEM coating unit before they were observed under the scanning electron microscope. The magnetism profile of MMO and naked MNPs were analysed through vibrating sample magnetometer (VSM) (Model: 7404, Lake Shore Cryotronic, Inc., Malaysia). Lastly, the surface charge of MNPs, MMO, POME and *M.oleifera* solution was measured by a zeta potential analyser (Model: Litesizer 500, Anton Paar, Austria). The zeta analysis was conducted at original pH. All characterizations were conducted at room temperature.

2.4. Comparative and regeneration studies

The coagulation performance of *M.oleifera* seed and optimized MMO was compared. The jar test conditions are similar as stated in Section 2.2.2. Besides that, the sedimentation kinetics was also performed and compared. After slow mixing, the sedimentation process was allowed to occur in 1L measuring cylinder. The flocs level was recorded for every minute for 60 min and the settling velocity was estimated.

Solvent elution method (dos Santos et al., 2018) was used to determine the feasibility of MMO regeneration. It consisted of separating the used MNPs from sludge resulting from the coagulation process by external magnetic assistance. The MNPs was then soaked with 20% ethanol solution for 10 min and distilled water before it was allowed to dry overnight. The dried MNPs were refunctionalized with the *M.oleifera* extract according to optimum experimental conditions and to be reused as a coagulant. The C–F-regeneration cycles were repeated 3 times.

3. Results and discussion

Efforts to increase process efficiency and performance of magnetic *Moringa oleifera,* which are the main concern of this study, are required prior to pilot and commercial scale application. The crystallite sizes of MNPs and MMO in the ultra-sonication synthesis were key factors in this novel assessment of magnetic attraction capability of the synthesized *Moringa oleifera* nanocomposite coagulant that could separate by an external magnetization after sedimentation takes place. The coagulant regeneration study highlighted an important criterion in evaluating the magnetic coagulant's potential in industrial wastewater treatment process especially with respect to POME. The statistical exploration of the interacting factors in the synthesis of the MMO provided the optimum synthesis conditions for optimum yield.

3.1. Model development and regression analysis

Prior to determination of optimum conditions, selection of model that have the best fitting are crucial as this ensures accuracy between predicted and experimental values. Based on the experimental results, the sequential model sum of squares (MSS) test was carried out, for all response variables, quadratic model shows the best model for data fitting. Among the various model types, the quadratic model gives the lowest standard deviation (1.68 ± 0.94) and highest R^2 value (0.9953 ± 0.0029). This result reflects that the predicted values were the most accurate, and closer to actual values utilizing quadratic model.

The analysis of variance (ANOVA) was used to explain the significant effect of mass fraction of MNPs and ultrasonic-synthesis conditions of MMO, as shown in Table S3 (Supplementary Materials). In this study, analysis using F-test revealed that all the models for TSS, colour, COD removal as well as SVI were significant at 95% confidence level ($p \leq 0.05$). Moreover, the terms are considered insignificant if the *p*-value is greater than 0.1 (Huzir et al., 2019). Based on Table S3, as for linear terms, the effect of sonication time shows an insignificant effect ($p > 0.1$) towards TSS and colour removals. This is attributed to the fact that at shorter sonication time, the ultrasound manages to maintain the reactivity of amide/carboxyl and Fe-O as a result of a continuous formation of cavitation bubbles of the coagulant surfaces. As for quadratic terms, all variables affect the models except for colour removal, the mass fraction of MNPs plays the least significance as well as sonication time for developed COD removal's model. The interaction terms between sonication time and sonication temperature shows insignificant effect towards colour and COD efficiency while the rest play a significant role in regressions. From the level of significance of the regression coefficient, it can be concluded that mass fraction of MNPs and sonication temperature proved to become the most influential single factor for all design responses. Meanwhile, sonication time gave the least responsive effect throughout the synthesis of MMO.

The statistical parameters from the ANOVA of these regression models was further demonstrated as shown in Table S4 (Supplementary Materials). The result shows that the model obtained a high R^2 for all responses, indicating desirable

correlation and a good quadratic fit for the model. R^2 should be more than 0.8 to ensure suitability and reasonable model in executing prediction of experimental outcomes (Xu et al., 2017). Hence, the models obtained (Table S3) are acceptable and can be used in predicting responses with an adequate accuracy and confidence level. The models also show a close figure between the predicted determination coefficient (Pred R^2) and the adjusted determination coefficient (Adj R^2). This concludes that the Pred R^2 of all these models were in reasonable agreement with the Adj R^2. In addition, a high value of Adj R^2 indicates the capability of the regression to satisfactorily describe the system behaviour within the ranges of operating variables.

The coefficient of variation (CV) is a term used to measure the reproducibility of the model. From Table S4, the CV values for all responses were less than 10%. According to (Bhatia et al., 2007; Li et al., 2010), a model is considered to be reasonably reproducible if its CV was at most 10%. These small CV might be due to the small standard deviation, because CV is a ratio of standard deviation to mean value. Another statistical tool to describe model adequacy is adequate precision (AP) which measures the signal to noise ratio (Teh et al., 2014). AP higher than 4 indicates desirable outcome and from the results, all response variables have adequate signal, because the AP is more than 4. In addition, after considering the significant terms, deduced models are shown in Table S5 (Supplementary Materials). The positive sign of terms in the model equations imply the appearance of synergistic effect between mutual interactions or individual effect while negative sign imply a reversal effects (Kakoi et al., 2017).

To further evaluate the prediction capability of the models, the plot of predicted versus actual data for each response is illustrated (Fig. 1). It is apparent that the prediction model of all responses is satisfactory as most of the points fall near to the line and corroborates the high R-value generated. In overall, the quadratic polynomial models used in this study can be used to navigate the design space.

3.2. Interaction of variables

To further understand the interactive effects of the independent variables on the dependent variable, the 3D surface graph and contour plots were analysed from the models developed and this lead to the conclusion on the optimum synthesis conditions of MMO coagulant. The plots were constructed according to a function of two variables at a time while keeping the remaining variables at zero level.

3.2.1. Effects of mass fraction of MNPs and sonication time

The relationship between mass fraction of MNPs (A) and sonication time (B) during synthesis of MMO is represented in Fig. 2. Their mutual interaction on TSS, colour, COD removal and SVI was compared while keeping sonication temperature at 55 °C. For all responses except for SVI model, it can be seen that mass fraction of MNPs gives more significant impact rather than sonication time. From the ANOVA table (Table S3) the F-value of mass of MNPs versus sonication time showed that the amount of MNPs was more significant than sonication time for the removal of TSS, colour and COD. The same trend was also observed for removal of colour and COD whereby the F-value of MNPs were 476.05 for colour and 64.11 for COD removal efficiencies, respectively, which much higher compared to F-value of sonication time, 0.78 and 64.11 for colour and COD removal, respectively. Unlike TSS, colour and COD removal, the F-value for sonication time (3814.81) are much higher than mass fraction of MNPs (593.3) nevertheless both factors show a significant impact to the model ($p<0.0001$).

Elliptical contours were obtained for TSS and SVI as shown in Fig. 2(a) and (d), respectively, which indicates a strong interaction between mass fraction of MNPs and sonication time (Fig. 2(a)). The TSS removal was achieved up to 80% at a MNPs dosage between 0.4 wt% and 0.6 wt% and a sonication time of around 30.5 min. Likewise, a maximum SVI was achieve at 0.6 wt% of MNPs dosage as well as 30.5 min of sonication time. The reason for this trend is that MNPs have high reactive and large surface-to-volume ratio, which can promote binding efficiency (Hwang and Han, 2015). However, the TSS removal and SVI performance is deficit as dosage of MNPs and sonication time is prolonged. This is because the protein interaction will not be efficient if the active site provided by the MNPs were masked by other contaminants in wastewater (Lakshmanan and Kuttuva Rajarao, 2014). As less protein deposited on MNPs surface there is less opposite charge available to destabilize colloidal suspension in POME.

Unlike TSS and SVI, colour and COD removal as shown in Fig. 2(b) and (c) shows a different trend. The planar pattern produced for colour removal model as shown in Fig. 2(b) indicated that in order to attain highest colour removal, a maximum mass fraction of MNPs and longest sonication time is required to obtain approximately 45.5% colour removal. The same trend is also shown by COD model in Fig. 2(c), an estimate COD removal of around 75% could be achieved at the highest range of MNPs dose (more than 0.6 wt%) and sonication time exceeding 30.5 min. The aromatic/aliphatic carboxyl or hydroxyl of organic matter and tannin–lignin-components could react with more of Fe-OH/Fe-OH$^+$ of MNPs via hydrogen bonding and ligand exchange surface complexing reactions, and this partially contributed to the relative high COD and colour removal (Lv et al., 2019). Limiting *M.oleifera* solution, increasing mass fraction of MNPs could be regard as adsorbent in MMO C–F system enhancing removal of organic matters.
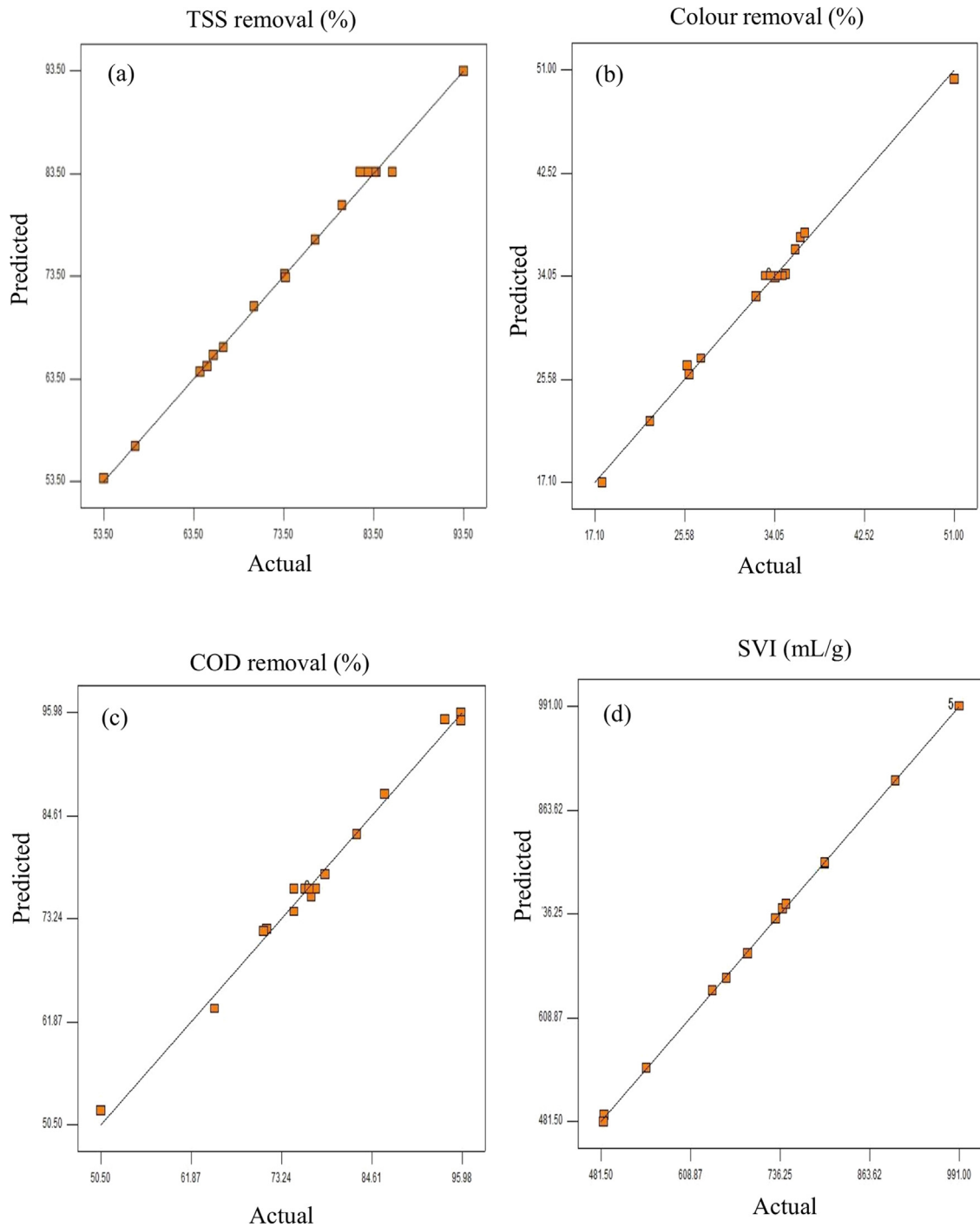
Fig. 1. Predicted versus actual plot for (a) TSS; (b) colour; (c) COD; (d) SVI.

3.2.2. Effects of mass fraction of MNPs and sonication temperature

The mutual interactions between mass fraction of MNPs (A) and sonication temperature (C) on TSS, colour, COD and SVI, at constant sonication time of 30.5 min are illustrated in Fig. 3. The results revealed that the effect of mass fraction of MNPs outweighs the effect of sonication temperature for only certain responses. The F-value of mass fraction of MNPs was higher than sonication temperature for both TSS (259.31 versus 113.56) and colour (476.05 versus 123.88) removal, suggesting that MNPs was the impactful variable during synthesis of MMO as well as for TSS and colour removal during
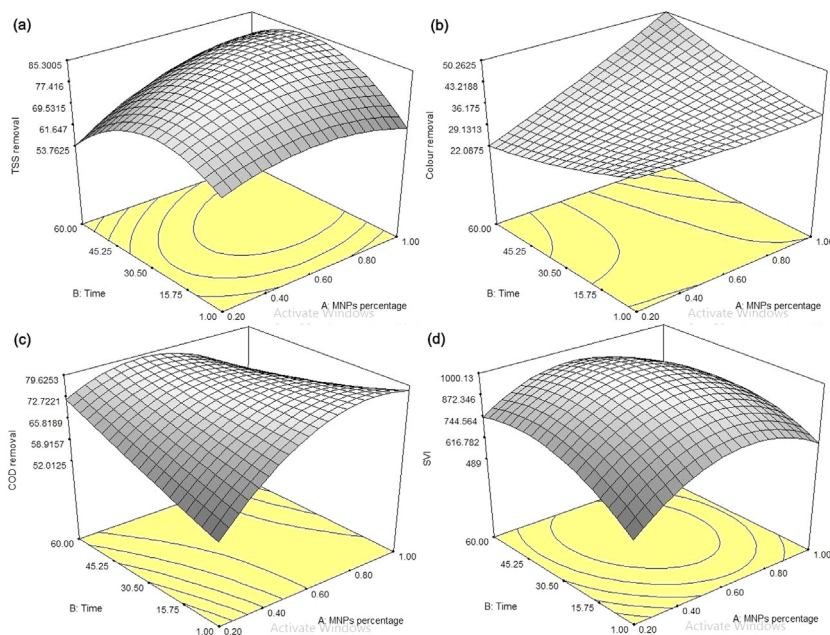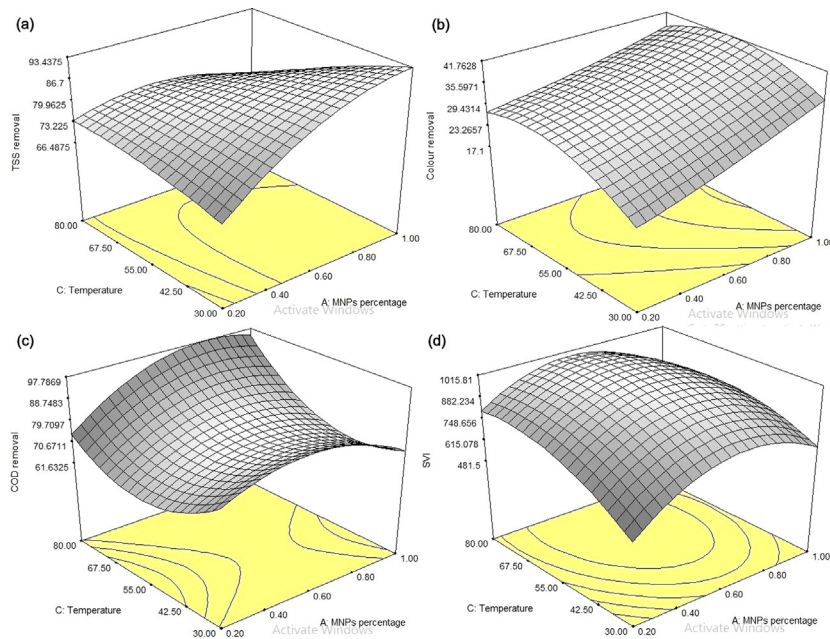
Fig. 2. Three-dimensional response surface plot for (a) TSS removal, (b) colour removal, (c) COD removal and (d) SVI as a response of interaction between mass fraction of MNPs (A) and sonication time (B).

coagulation process. From Fig. 3(a) the maximum TSS removal (around 80%) can possibly achieved at the dosage of MNPs more than 0.6 wt% and sonication temperature around zero level (55 °C). The same fashion was observed for colour model as showed in Fig. 3(b) in order to target 40% removal. With increasing kinetic (effect of temperature) and acoustic (effect of ultrasound) energy, MNPs became easier to combine with the *M.oleifera* extract of the coagulant to form a more compact magnetic coagulant (Liu et al., 2017). Moreover, mutual attraction between magnetic particles was enhanced, thus increasing the number of particles that was aggregated by MMO into large aggregation, ultimately leading to a good coagulation effect respectively.

Even though mass fraction and sonication temperature contribute significant variables towards COD removal and SVI models based on *p*-value <0.0001, sonication temperature portrayed considerable factor compared to mass fraction of MNPs. From Table S3, the F-value for sonication temperature for both COD removal and SVI were 100.4 and 8422.89, respectively compared to F-values of 64.11 and 593.3 corresponding to mass fraction of MNPs in the same models. Saddle pattern shown in Fig. 3(c) indicates COD reduction could be achieved at two points of MNPs dosage which is either around 0.5 wt% or 0.8 wt% but at fixed optimum sonication temperature of 55 °C. At these conditions a maximum COD removal of 75% could be attained. For SVI model, as shown in Fig. 3(d), target of minimal SVI (approximately 574.19 mL/g) can be hit if the process was conducted at the lowest mass fraction of MNPs (0.2 wt%) as well as at the lowest sonication temperature (30 °C). At this stage, particles of *M.oleifera* at fixed volume rely on the kinetic energy in order for complete coating of the MNPs particles in a limited span of time in order to maximize the coagulation performance in removing organic matters in the POME. On the other hand, as the mass fraction of MNPs increases with increasing temperature, MNPs was easier to be oxidized, resulting in the weak magnetism of MMO (Wang et al., 2017). Another possible reason is that excessive magnetic intensity and MMO dosage will make the magnetic particles settle very quickly to achieve a full contact reaction with pollutants (Li et al., 2016) which limits the COD removal as well increasing amount of sludge.

3.2.3. Effects of sonication time and sonication temperature

Fig. 4 depicts the effects of varying sonication time and sonication temperature on TSS, colour, COD and SVI removal efficiencies at constant conditions of 0.6 wt% of MNPs dosage. It can be deduced that effect of sonication time are more impingement on TSS, colour, COD and SVI responses rather than sonication time as shown by F-value of individual variables in Table S3. Equally, based on 3D-response surface plot in Fig. 4 most of the models illustrate an elliptical pattern and shows that responses are mostly influenced by sonication temperature as compared to sonication time. At constant amount of MNPs (zero level) the TSS removal can be maximized to 80% when MMO is synthesized at sonication temperature around 67.5 °C for 30.5 min as showed in Fig. 4(a) and at same conditions an approximate 36% of colour removal is achievable (Fig. 4(b)). As for COD removal in Fig. 4(c), selection of optimum sonication temperature affected the performance, as varying sonication time gives no effect on the COD reduction. A maximum 95% COD removal can be achieved if the synthesis process is conducted at 80 °C regardless of sonication time. Additionally, in order to achieve a

Fig. 3. Three-dimensional response surface plot for (a) TSS removal, (b) colour removal, (c) COD removal and (d) SVI as a response of interaction between mass fraction of MNPs (A) and sonication temperature (C).

minimum production of sludge (in term of SVI), the model expected to produce less than 550 mL/g of SVI through 1 min and around 42 °C of sonication time and sonication temperature respectively, during synthesis of MMO coagulant.

In general, all responses show better performances as temperature and reaction time was increased. This can be explained by effective collision phenomena. Increasing sonication temperature increases the kinetic energy between MNPs and *M.oleifera* solution particles and prolonged sonication time gives more advantages as these give the particles adequate time to aggregate to each other. As more particles collide with each other, collision cause reaction (effective collision) between polymers from *M.oleifera* solution to be attach to MNPs as main core. This high yield of MMO provide more charge (from *M.oleifera* solution) and surface area (from MNPs) for entrapment and adsorption of pollutants from POME on MMO during execution of coagulation process and this results in higher TSS, colour, COD removal as well as SVI production.

### 3.3. Attaining optimum condition and validation of model

After analysing and finalizing the quadratic models, design optimization was executed and the optimum operating conditions were determined. The outcome of this optimization is tabulated in Table S6 (Supplementary Materials), which provides the optimum values of MNPs (in wt%), sonication time and sonication temperature to yield the highest percentage removals of TSS, colour, COD and least SVI. Using the optimum conditions, the experiment was repeated three times and the responses were compared to the predicted values to verify the accuracy and stability of the models. From Table S6, the error percentage was observed for SVI at 9.7%, followed by COD at 6.8% and the least deviation was obtained by TSS, which is only 0.3%. For a study on experimental design optimization employing RSM, a percentage error below 10% is generally acceptable if the nature of the experiment involves several fluctuating situations, provided the experimental values are within 95% prediction intervals of the model (Hejazi et al., 2014). From the finding, it can be concluded that the model for TSS, colour, COD and SVI was verified and acceptable despite minor error. The results in this study were compared with previous reports and presented in Table S7 (Supplementary Materials).

### 3.4. Characterization of optimized MMO coagulant

3.4.1. FTIR spectra analysis

The optimized preparation conditions of MMO coagulant as well as MNPs powder were characterized using FTIR and XRD analysis. The spectra are shown in Fig. 5. The IR-spectra for MNPs shows a sharp intensity at 569 cm^{-1} and represents the Fe-O bond of magnetic material (Mateus et al., 2018a,b). Zheng et al. (2011) in their study mentioned that vibration peak between 550 and 634 cm^{-1} corresponds to magnetite characteristics. Similarly, the same band around 582 cm^{-1} was observed in MMO spectra. The bands are slightly different from naked MNPs because of interruption related to association
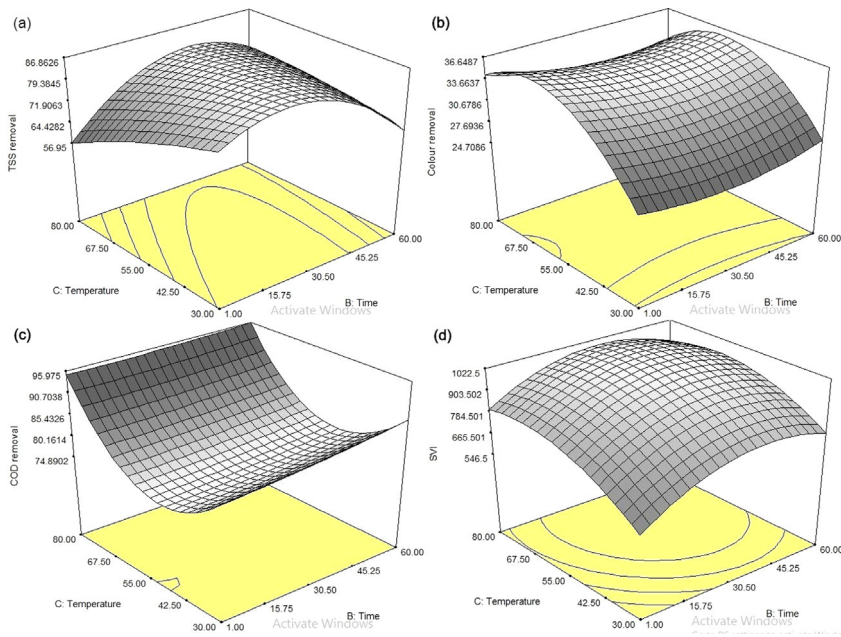
Fig. 4. Three-dimensional response surface plot for (a) TSS removal, (b) colour removal, (c) COD removal and (d) SVI as a response of interaction between sonication time (B) and sonication temperature (C).
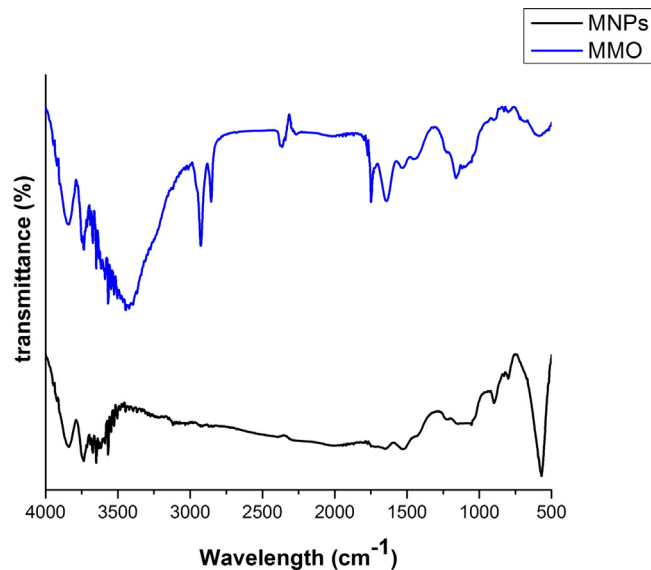
Fig. 5. FTIR analysis of MNPs and MMO.

with vibrations of the groups $Fe^{2+}-O^2$ and the symmetric deformation of the octahedral site when other materials are introduced during synthesis of MMO (Mateus et al., 2018a,b). Besides, the relative transmittance weakens for MMO spectra in this area because the functional groups from *M.oleifera* extract solution interact with the MNPs material leading to a lesser vibrational frequency (Kgatitsoe et al., 2019). Moreover, the characteristics of biomass source, which is mostly contributed by *M.oleifera* were still found in MMO spectra. Peak around 2926 cm^{-1} represent a C – H bond stretching associated with fatty acid (dos Santos et al., 2018). The band around 1640 cm^{-1} was attributed to C – *N* showing the presence of amide group in the protein MMO coagulant (Reck et al., 2019; Triques et al., 2020).
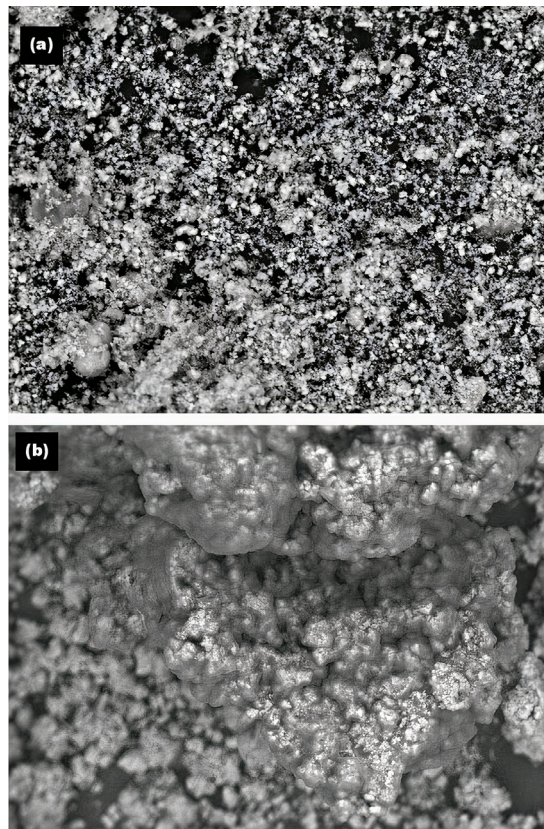
Fig. 6. Scanning electron micrograph of (a) MNPs and (b) MMO (Magnification 2000×).

3.4.2. SEM analysis

The morphology of the synthesized coagulant was analysed by SEM. Micrographs of MMO as well as MNPs samples are presented in Fig. 6. It is observed that MNPs (Fig. 6(a)) presents as agglomerates due to the ferromagnetic characteristics of the obtained material. This is because the MNPs had stronger magnetic dipole–dipole forces and hence leads to the formation of larger clusters (Ju et al., 2015). Meanwhile, the micrograph of MMO in Fig. 6(b) shows reduced agglomeration of MNPs. This is probably due to the introduction of ultrasonic force, which maximizes the dispersion of MNPs for better functionalization with *M.oleifera* solution. It was also observed that MNPs was surrounded with a carbonic material (grey mass) in MMO micrograph, possibly attributable to the proteins and other compounds from the *M.oleifera* (Mateus et al., 2018a,b). The MNPs had an average particle size of 20 nm while the MMO were well dispersed with an average size of 13 nm. This has proven that ultrasonic force could prevent the agglomeration of MNPs and resulted in smaller, well-dispersed clusters in the synthesis of MMO coagulant.

3.4.3. XRD analysis

Fig. 7 shows the sharp and narrow peaks of crystalline profiles of XRD for the both MNPs and MMO. An obvious observation in the diffractogram is that the *M.oleifera* functionalized MNPs is similar to that of the bare MNPs. This indicates that the modification process with the *M.oleifera* and introduction of ultrasonication did not significantly alter the core structure of the MNPs. This finding is also in agreement with the report of Kgatitsoe et al. (2019). For both patterns, a clear diffraction peaks at around 2θ of 18.3°, 35.4°, 37.1°, 43.1°, 57.0 and 62.6° were identified and they represent the magnetic planes (111), (220), (311), (400), (511) and (440). The highest intensity observed for the 311 plane followed by the 400 plane corresponds to Fe^{3+} ions in magnetite that is in tetrahedral and octahedral sites as well as in inverse spinel crystalline structure in cubic form (Mateus et al., 2018a,b; Santos et al., 2016).

The approximate average crystallite sizes of MNPs and MMO were 20 nm and 47 nm, respectively after Scherrer equation was applied. The increment in the crystal size after functionalization is associated with the presence of soluble protein and other compounds present in the *M.oleifera* extract (Reck et al., 2019). The synthesized MMO coagulant has ferromagnetic properties due to the crystalline size below 50 nm and black in colour (Cheng and Zheng, 2014).
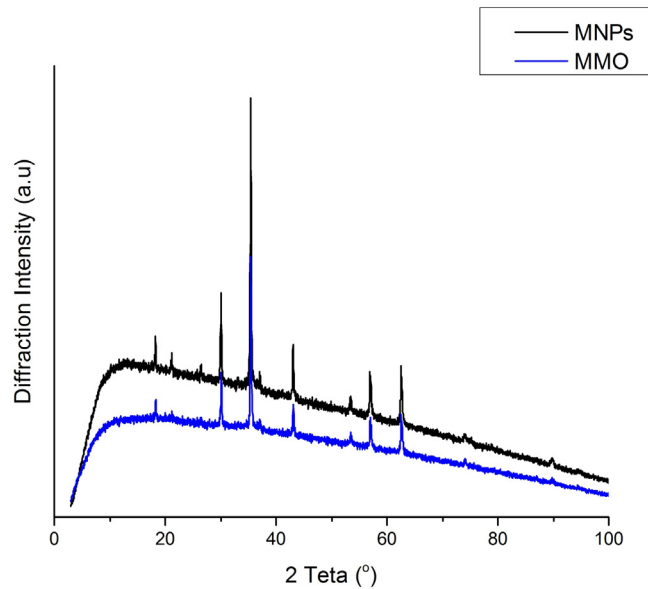
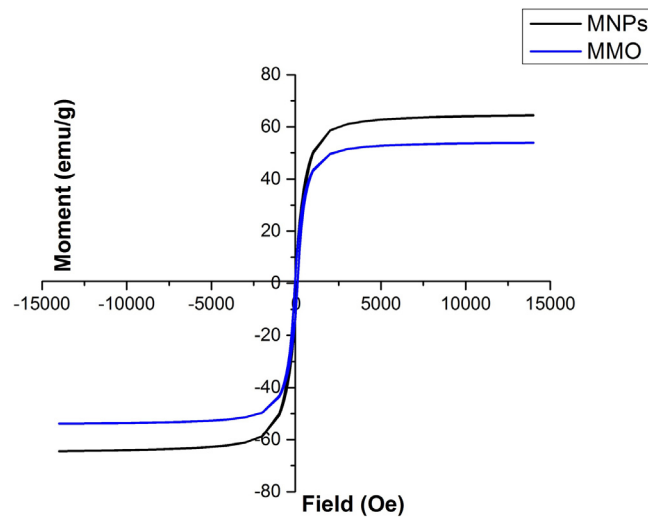**Fig. 7.** X-ray diffractogram of (a) MNPs and (b) MMO.

Fig. 8. Magnetic hysteresis loop of MNPs and MMO.

3.4.4. VSM analysis

The magnetic properties of the MNPs and synthesized MMO were determined by employing the VSM at room temperature. The plots of magnetization versus magnetic field for both MNPs and MMO are presented in Fig. 8.

Initially, both materials had zero moment or magnetization but when the current was applied and kept increasing, the field intensity also increased until each of the materials achieved their on saturation point. MNPs shows a moment saturation (M_s) at 64.10 emu/g meanwhile for MMO, the M_s appeared at 53.85 emu/g. Saturation occurs when on increasing the current, dipole moment or the molecules of the magnetic materials align itself in one direction. The reduction of M_s between MNPs and MMO are due to the composite of nonmagnetic (*M.oleifera*) element on the MNPs surface and thus slightly reduced the magnetic strength of the composite MMO. With further decrease in the magnetic field, both MNPs and MMO left a magnetic residual or retentivity (M_r) (define as the remaining magnetic moment when field is equal to zero) at point 9.0 emu/g and 8.0 emu/g, respectively. Thus, to eliminate the residual magnetic moment, an electric current is to be applied but in opposite direction. At this stage, MNPs and MMO required an applied magnetic field of 75.8 Oe and 75.6 Oe in order to eliminate the remaining magnetic moment in each material. This was named as coercivity point (defined as a force required to demagnetize a magnetic material, moment = 0). These characteristics imply that MNPs and MMO show ferromagnetic behaviour because according to Okoli et al. (2012), a ferromagnetic material
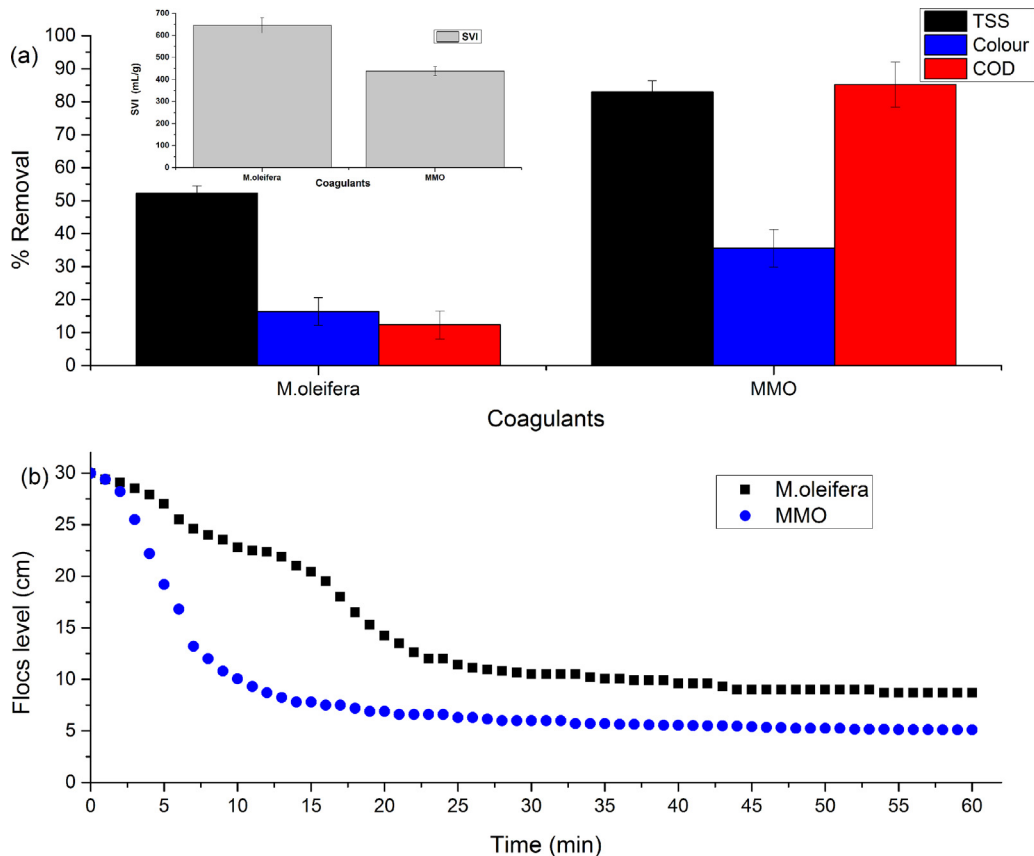
11

Fig. 9. (a) Coagulation performance and (b) sedimentation kinetics of *M.oleifera* and MMO.

have a high saturation of magnetization and force of coercivity, and retentivity close to zero, as can be observed in this study. This result is also supported by the XRD analysis. From the magnetic study, it can be deducted that this feature is ideal for the proposed application as it allows for magnetic attraction and the synthesized nanocomposite coagulant could simply be separated by an external magnetic force after sedimentation takes place (Reck et al., 2019).

3.4.5. Zeta potential analysis

Zeta potential is a key parameter to understanding electrostatic interactions between particles in a solution. Table S8 (Supplementary Materials) shows a zeta potential of each samples analysed at original pH. In natural pH, the surface of MNPs shows a negative charge potential due to the dissociation of iron and hydroxyl group (Fe-OH) followed by the formation of Fe-O$^-$ (Yu and Chow, 2004). The presence of the hydroxyl group on the MNPs particle surface was also confirmed by infrared measurement as describe later. According to dos Santos et al. (2018), the zero potential charge of magnetite is found at pH 4.35. Above this pH, the material surface is negatively charged and it is in agreement with this study. As expected, POME also gives a negatively charged surface due to the presence of highly concentrated hydroxide ion (Zahrim et al., 2017). High negatively charge colloid leads to high repulsion between the POME colloids. Therefore, cationic coagulant should be applied to destabilize the colloid.

The zeta potential for *M.oleifera* solution and MMO present similar behaviour, showing positive charge at pH near neutral. It was also identified that *M.oleifera* solution presents more positive zeta potential than functionalized *M.oleifera*. It could be explained by the presence of cationic protein responsible for coagulant characteristic of *M.oleifera*. When *M.oleifera* solution was functionalized with MNPs, the *M.oleifera* soluble protein attached to the surface of the MNPs because carboxylic acids have a high affinity for metallic oxides (Reck et al., 2019). The cationic *M.oleifera* solution thus reduced the negatively charged surface of MNPs during functionalization and produces a MMO with net positive surface charge. Due to difference in surface charge between MMO and POME, it is expected that charge neutralization is the dominant mechanism when C–F process takes place.

3.5. Comparative study

The coagulation performance of MMO was also compared with *M.oleifera* and the results as illustrated in Fig. 9(a). It can be seen that the presence of MNPs has improved the coagulation performance in removing pollutants from POME as well
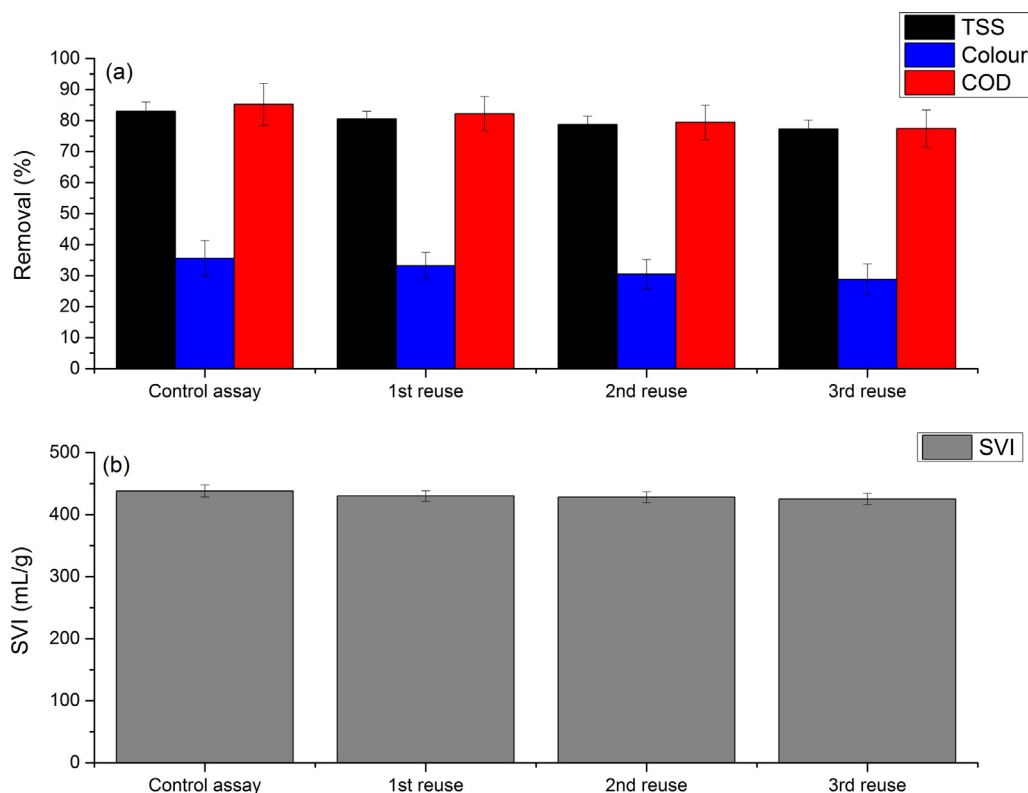
Fig. 10. (a) Removal parameters of TSS, colour, COD and (b) SVI in coagulation process using regenerated MMO at optimum experimental conditions.

as manage to minimize the sludge production. Coagulation by *M.oleifera* seed however shows an unproductive activity in removing pollutants. The removals of TSS, colour and COD are only 52.22, 16.42, 12.33%, which is much lower compared to coagulation performance by MMO (also stated in Table S6). Due to the instability, Fe^{2+} in MNPs made this ions protonated when exposed to solution rich in colloidal particles (Bakhteeva et al., 2019; Chen et al., 2019). This enhances the charge neutralization mechanism during coagulation process thus reflecting better pollutant removals. In addition, the sludge produced by *M.oleifera* coagulant were 645 mL/g which is about 32% higher than the sludge produced by MMO coagulation. It is recommended that *M.oleifera* required more dosage in order to improve the removals however it will affect the sludge production and the presence of MNPs, is proven to improve the coagulation performance of MMO as well as minimized the sludge production. This is probably due to the production of compact sludge (Kgatitsoe et al., 2019).

The sedimentation kinetics of flocs between *M.oleifera* and MMO was also conducted in within 60 min settling time as show in Fig. 9(b). A sharp drop of MMO's flocs can be seen in within 15 min before it reached stable settling time. Settling time by *M.oleifera* however consumed longer time before flocs reached equilibrium settling time. It was estimated that the settling speed coagulation by MMO and *M.oleifera* were 1.64 and 0.67 cm/min, respectively. This phenomenon indicates that *M.oleifera* protein functionalized with MNPs has resulted in denser flocs due to more embedded coagulant agents incorporating magnetic properties of MNPs. This approach gave great advantages especially on minimizing the reaction time.

3.6. Magnetic coagulant regeneration

The coagulant regeneration is an important criterion in evaluating the magnetic coagulant's potential in industrial wastewater treatment process. Fig. 10(a) reveals that the MMO performance in removing TSS, colour, COD decreased from 83, 35.6 and 85.2% in the first use to 77.3, 28.8 and 77.4% on the third reuse, respectively. The regeneration seem to produce small impact on the SVI whereby there is only 3% (13 mL/g) differences from the control assay to third reuse assay as illustrated in Fig. 10(b). The reduction in the MMO efficiency could be a consequence of the mass loss during each step. Solvent elution by ethanol helped in removing residual synthesis impurities from MNPs, and consequently leads to higher available MNPs surface area thus providing greater functionalization with active compound of *M.oleifera* extract (dos Santos et al., 2018). This action probably prevent the MMO performance from gradual drop in pollutant removals of POME. Other studies in utilization of MMO regeneration also show comparable results. For instance, Triques et al. (2020) obtained a 80% turbidity reduction after second reuse of MMO when applied on dairy wastewater. Reusability test of

MMO on raw water collected from the Pirapó River, Brazil showed a promising turbidity, apparent colour and $UV_{254\ nm}$ with approximately 90, 85 and 43% removals after third reuse, respectively (Mateus et al., 2018a,b). The finding of this study indicates the high stability of MMO upon repeated usage, which is vital to reduce the material cost and minimize the secondary pollution.

4. Conclusions

This study addressed the influence of sonication conditions in the fabrication of MMO coagulant. The synthesis process was optimized using the RSM. The mass fraction of MNPs (0.2–1.0 wt%), sonication time (1–60 min) and sonication temperature (30–80 °C) were selected as the main parameters and the optimum synthesis conditions were selected based on the highest TSS, colour, COD removal as well as minimum SVI value when coagulation performance for the treatment of POME was conducted. The RSM results indicate that 1.0 wt% of MNPs, 2.35 min and 50 °C was the optimal mass fraction of MNPs, sonication time and sonication temperature, respectively in order to obtain 83.3%, 28.1%, 85.2% removal of TSS, colour, COD, respectively as well as 485 mL/g of SVI value. From the characterization analysis it shows that *M.oleifera* was successfully functionalized with MNPs and exhibited ferromagnetic properties for better separation process. This paper shows the time efficiency in utilizing sonication technology for the fabrication of MMO which portrayed a better coagulation performance when compared to already published works.

CRediT authorship contribution statement

Mohamed Hizam Mohamed Noor: Conceptualization, Validation, Writing – original draft. **Muhammad Faiz Zaim Mohd Azli:** Methodology, Investigation, Writing – original draft. **Norzita Ngadi:** Writing – review & editing, Supervision, Funding acquisition. **Ibrahim Mohammed Inuwa:** Writing – review & editing , Visualization. **Lawal Anako Opotu:** Writing – review & editing, Data curation. **Mahadhir Mohamed:** Writing – review & editing, Supervision.

Declaration of competing interest

The authors declare that they have no known competing financial interests or personal relationships that could have appeared to influence the work reported in this paper.

Acknowledgement

Appendix A. Supplementary data

Supplementary material related to this article can be found online at https://doi.org/10.1016/j.eti.2021.102191.

References

APHA, xx., AWWA, xx., WEF, xx., 1992. Standards Methods of Examination of Water and Wastewater. IWA Publishing, Washington, DC.

Bakhteeva, I.A., Medvedeva, I.V., Filinkova, M.S., Byzov, I.V., Zhakov, S.V., Uimin, M.A., Yermakov, A.E., 2019. Magnetic sedimentation of nonmagnetic TiO_2 nanoparticles in water by heteroaggregation with Fe-based nanoparticles. Separation and Purification Technology 218, 156–163.

Baptista, A.T.A., Coldebella, P.F., Cardines, P.H.F., Gomes, R.G., Vieira, M.F., Bergamasco, R., Vieira, A.M.S., 2015. Coagulation–flocculation process with ultrafiltered saline extract of Moringa oleifera for the treatment of surface water. Chem. Eng. J. 276, 166–173.

Villaseñor Basulto, D.L., Astudillo-Sánchez, P.D., del Real-Olvera, J., Bandala, E.R., 2018. Wastewater treatment using Moringa oleifera Lam seeds: A review. J. Water Process Eng. 23, 151–164.

Bhatia, S., Othman, Z., Ahmad, A.L., 2007. Pretreatment of palm oil mill effluent (POME) using Moringa oleifera seeds as natural coagulant. J. Hard Mater. 145 (1–2), 120–126.

Camacho, F.P., Sousa, V.S., Bergamasco, R., Ribau Teixeira, M., 2017. The use of Moringa oleifera as a natural coagulant in surface water treatment. Chem. Eng. J. 313, 226–237.

Chen, X., Zheng, H., Xiang, W., An, Y., Xu, B., Zhao, C., Zhang, S., 2019. Magnetic flocculation of anion dyes by a novel composite coagulant. Desalin. Water Treat. 143, 282–294.

Cheng, G., Zheng, S.-Y., 2014. Construction of a high-performance magnetic enzyme nanosystem for rapid tryptic digestion. Sci. Rep. 4, 6947.

Dai, J., Yu, B., Yang, L., Zhang, Y., Liu, Z., Liu, P., 2020. Microstructure and mechanical properties of ultrasonically assisted brazing of dissimilar Cu–Al alloys. Science of Advanced Materials 12 (5), 733–739.

dos Santos, T.R.T., Silva, M.F., de Andrade, M.B., Vieira, M.F., Bergamasco, R., 2018. Magnetic coagulant based on Moringa oleifera seeds extract and super paramagnetic nanoparticles: optimization of operational conditions and reuse evaluation. Desalin. Water Treat. 106, 226–237.

Garcia-Fayos, B., Arnal, J.M., Sancho, M., Rodrigo, I., 2016. Moringa oleifera for drinking water treatment: influence of the solvent and method used in oil-extraction on the coagulant efficiency of the seed extract. Desalin. Water Treat. 57 (48–49), 23397–23404.

Garde, W.K., Buchberger, S.G., Wendell, D., Kupferle, M.J., 2017. Application of Moringa Oleifera seed extract to treat coffee fermentation wastewater. J. Hard Mater. 329, 102–109.

Hejazi, T.H., Bashiri, M., Dı̇, J.A., Noghondarian, K., 2014. Optimization of probabilistic multiple response surfaces. Appl. Math. Model. 36 (3), 1275–1285.

Huzir, N.M., Aziz, M.M.A., Ismail, S.B., Mahmood, N.A.N., Umor, N.A., Faua'ad Syed Muhammad, S.A., 2019. Optimization of coagulation-flocculation process for the palm oil mill effluent treatment by using rice husk ash. Industrial Crops and Products 139, 111482.

Hwang, J.H., Han, D.W., 2015. Optimization and modeling of reduction of wastewater sludge water content and turbidity removal using magnetic iron oxide nanoparticles (MION). J. Environ. Sci. Health 50 (13), 1307–1315.

Ju, S., Liu, M., Yang, Y., 2015. Preconcentration and determination of Cadmium, lead, and cobalt inmoringa oleifera(moringaceae) using magnetic solid-phase extraction and flame atomic absorption spectrometry. Anal. Lett. 49 (4), 511–522.

Kakoi, B., Kaluli, J.W., Ndiba, P., Thiong'o, G., 2017. Optimization of Maerua Decumbent bio-coagulant in paint industry wastewater treatment with response surface methodology. J. Cleaner Prod. 164, 1124–1134.

Kgatitsoe, M.M., Ncube, S., Tutu, H., Nyambe, I.A., Chimuka, L., 2019. Synthesis and characterization of a magnetic nanosorbent modified with Moringa oleifera leaf extracts for removal of nitroaromatic explosive compounds in water samples. J. Environ. Chem. Eng. 7 (3), 103128.

Lakshmanan, R., Kuttuva Rajarao, G., 2014. Effective water content reduction in sewage wastewater sludge using magnetic nanoparticles. Bioresour. Technol. 153, 333–339.

Lee, C.S., Robinson, J., Chong, M.F., 2014. A review on application of flocculants in wastewater treatment. Process Safety and Environmental Protection 92 (6), 489–508.

Li, S., Wang, X.-m., Zhang, Q.-l., 2016. Dynamic experiments on flocculation and sedimentation of argillized ultrafine tailings using fly-ash-based magnetic coagulant. Trans. Nonferr. Met. Soc. China 26 (7), 1975–1984.

Li, H., Zhou, S., Sun, Y., Lv, J., 2010. Application of response surface methodology to the advanced treatment of biologically stabilized landfill leachate using Fenton's reagent. Waste Management 30 (11), 2122–2129.

Liu, P.-R., Wang, T., Yang, Z.-Y., Hong, Y., Hou, Y.-L., 2017. Long-chain poly-arginine functionalized porous Fe3O4 microspheres as magnetic flocculant for efficient harvesting of oleaginous microalgae. Algal Research 27, 99–108.

Luo, D.-L., Qiu, T.-Q., Lu, Q., 2005. Ultrasound technology and its applications (I) ultrasound technology. Riyong Huaxue Gongye 35 (5), 323–326.

Lv, M., Zhang, Z., Zeng, J., Liu, J., Sun, M., Yadav, R.S., Feng, Y., 2019. Roles of magnetic particles in magnetic seeding coagulation-flocculation process for surface water treatment. Separation and Purification Technology 212, 337–343.

Mace, E., Montaldo, G., Osmanski, B.-F., Cohen, I., Fink, M., Tanter, M., 2013. Functional ultrasound imaging of the brain: theory and basic principles. IEEE Trans. Ultrason. Ferroelectr. Freq. Control 60 (3), 492–506.

Madrona, G.S., Serpelloni, G.B., Salcedo Vieira, A.M., Nishi, L., Cardoso, K.C., Bergamasco, R., 2010. Study of the effect of saline solution on the extraction of the Moringa oleifera seed's active component for water treatment. Water Air Soil Pollut. 211 (1–4), 409–415.

Mateus, G.A.P., Paludo, M.P., dos Santos, T.R.T., Silva, M.F., Nishi, L., Fagundes-Klen, M.R., Gomes, R.G., Bergamasco, R., 2018b. Obtaining drinking water using a magnetic coagulant composed of magnetite nanoparticles functionalized with Moringa oleifera seed extract. J. Environ. Chem. Eng. 6 (4), 4084–4092.

Mateus, G.A.P., dos Santos, T.R.T., Sanches, I.S., Silva, M.F., de Andrade, M.B., Paludo, M.P., Gomes, R.G., Bergamasco, R., 2018a. Evaluation of a magnetic coagulant based on Fe3O4 nanoparticles and Moringa oleifera extract on tartrazine removal: coagulation-adsorption and kinetics studies. Environ. Technol. 1–16.

Mohamed Noor, M.H., Lee, W.J., Mohd Azli, M.F.Z., Ngadi, N., Mohamed, M., 2021. *Moringa oleifera* extract as green coagulant for POME treatment: Preliminary studies and sludge evaluation. Materials Today: Proceedings 46, 1940–1947.

Okoli, C., Boutonnet, M., Järås, S., Rajarao-Kuttuva, G., 2012. Protein-functionalized magnetic iron oxide nanoparticles: time efficient potential-water treatment. J. Nanoparticle Res. 14 (10).

de Paula, H.M., de Oliveira Ilha, M.S., Sarmento, A.P., Andrade, L.S., 2018. Dosage optimization of Moringa oleifera seed and traditional chemical coagulants solutions for concrete plant wastewater treatment. J. Cleaner Prod. 174, 123–132.

Pecora, H.B., Dilarri, G., Mendes, C.R., Corso, C.R., 2018. Bioassays and coagulation studies using Moringa oleifera seeds for the removal of textile dyes. Water Sci. Technol..

Pham, T.D., Shrestha, R.A., Virkutyte, J., Sillanpää, M., 2013. Recent studies in environmental applications of ultrasound. J. Environ. Eng. Sci. 8 (4), 403–412.

Reck, I.M., Baptista, A.T.A., Paixão, R.M., Bergamasco, R., Vieira, M.F., Vieira, A.M.S., 2019. Protein fractionation of Moringa oleifera Lam. seeds and functionalization with magnetic particles for the treatment of reactive black 5 solution. Can. J. Chem. Eng..

Santos, T.R., Silva, M.F., Nishi, L., Vieira, A.M., Fagundes-Klen, M.R., Andrade, M.B., Vieira, M.F., Bergamasco, R., 2016. Development of a magnetic coagulant based on Moringa oleifera seed extract for water treatment. Environ. Sci. Pollut. Res. Int. 23 (8), 7692–7700.

Sudol, W., 2010. Ultrasound transducer and method for implementing flip-chip two dimensional array technology to curved arrays. Google Patents.

Teh, C.Y., Wu, T.Y., Juan, J.C., 2014. Optimization of agro-industrial wastewater treatment using unmodified rice starch as a natural coagulant. Industrial Crops and Products 56, 17–26.

Triques, C.C., Fagundes-Klen, M.R., Suzaki, P.Y.R., Mateus, G.A.P., Wernke, G., Bergamasco, R., Rodrigues, M.L.F., 2020. Influence evaluation of the functionalization of magnetic nanoparticles with a natural extract coagulant in the primary treatment of a dairy cleaning-in-place wastewater. J. Cleaner Prod. 243, 118634.

Wang, C., Wang, Y., Ouyang, Z., Shen, T., Wang, X., 2017. Preparation and characterization of polymer-coated Fe3O4 magnetic flocculant. Sep. Sci. Technol. 53 (5), 814–822.

Wongcharee, S., Aravinthan, V., Erdei, L., 2020. Removal of natural organic matter and ammonia from dam water by enhanced coagulation combined with adsorption on powdered composite nano-adsorbent. Environ. Technol. Innov. 17, 100557.

Wu, T.Y., Guo, N., Teh, C.Y., Wen Hay, J.X., 2013. Advances in Ultrasound Technology for Environmental Remediation. Springer, New York.

Xu, J., Long, Y., Shen, D., Feng, H., Chen, T., 2017. Optimization of Fenton treatment process for degradation of refractory organics in pre-coagulated leachate membrane concentrates. J. Hard Mater. 323 (Pt B), 674–680.

Yang, M., Jin, R., Wang, Z., Liu, J., Barua, R., Song, X., Zhang, M., 2020. Ultrasonic-induced enhancement in interfacial exchange coupling of composite ferrites via chemical co-precipitation. J. Alloys Compd. 820, 153429.

Yu, S., Chow, G.M., 2004. Carboxyl group (–CO 2H) functionalized ferrimagnetic iron oxide nanoparticles for potential bio-applications. J. Mater. Chem. 14 (18), 2781–2786.

Zahrim, A.Y., Dexter, Z.D., Joseph, C.G., Hilal, N., 2017. Effective coagulation-flocculation treatment of highly polluted palm oil mill biogas plant wastewater using dual coagulants: Decolourisation, kinetics and phytotoxicity studies. J. Water Process Eng. 16, 258–269.

Zheng, L., Su, W., Qi, Z., Xu, Y., Zhou, M., Xie, Y., 2011. First-order metal–insulator transition and infrared identification of shape-controlled magnetite nanocrystals. Nanotechnology 22 (48), 485706.

Zhou, Z., Yang, Y., Li, X., Li, P., Zhang, T., Lv, X., Liu, L., Dong, J., Zheng, D., 2018. Optimized removal of natural organic matter by ultrasound-assisted coagulation of recycling drinking water treatment sludge. Ultrasonics Sonochemistry 48, 171–180.

Zhou, Y., Zheng, H., Wang, Y., Zhao, R., Liu, H., Ding, W., An, Y., 2020. Enhanced municipal sludge dewaterability using an amphiphilic microblocked cationic polyacrylamide synthesized through ultrasonic-initiation: Copolymerization and flocculation mechanisms. Colloids Surf. A 594, 124645.